Counter Cross-flow Evaporator Geometries for Supercritical Organic Rankine Cycles

Ali H. Nejad[a], Kivanc Ekici[a,*], Adrian S. Sabau[b,a], Adrian Bejan[c], Rao V. Arimilli[a]

[a] *Mechanical, Aerospace and Biomedical Engineering, The University of Tennessee, Knoxville, TN 37996, USA*
[b] *Computational Sciences and Engineering Division, Oak Ridge National Laboratory, Oak Ridge, TN 37830, USA*
[c] *Mechanical Engineering and Materials Science, Duke University, Durham, NC 27708, USA*

Abstract

With recent advancements in advanced manufacturing techniques, it is now possible to fabricate complex geometries that take advantage of well known principles of heat transfer. Therefore, unconventional configurations to enhance effectiveness beyond conventional designs can now be considered for practical application. Thermal performance and overall cost of a new design of heat exchangers in counter cross-flow configurations are studied using a simplified but accurate computational method. The new heat exchanger design was introduced and studied previously for a cross-flow configuration by

☆ *Notice: This submission was sponsored by a contractor of the United States Government under contract DE-AC05-00OR22725 with the United States Department of Energy. The United States Government retains and the publisher, by accepting the article for publication, acknowledges that the United States Government retains a non-exclusive, paid-up, irrevocable, world-wide license to publish or reproduce the published form of this manuscript, or allow others to do so, for United States Government purposes. The Department of Energy will provide public access to these results of federally sponsored research in accordance with the DOE Public Access Plan (http://energy.gov/downloads/doe-public-access-plan).*

*Corresponding author.

Email addresses: ali@utk.edu (Ali H. Nejad), ekici@utk.edu (Kivanc Ekici), sabaua@ornl.gov (Adrian S. Sabau), abejan@duke.edu (Adrian Bejan), arimilli@utk.edu (Rao V. Arimilli)

Sabau et al. [1, 2]. This new design concept uses multi-scale configurations with successive plenums for the working fluid. At the smallest scale the tubes are sized to be equal to the hydraulic entrance length of the inside fluid, in accord with constructal design. Results indicate that compared to the earlier cross-flow configuration, the counter cross-flow arrangement improves the thermal performance of the heat exchanger by as much as 17% and lowers the total cost by as much as 14%.
Keywords: Counter cross-flow heat exchanger, Thermal performance, Constructal, Cost.

Nomenclature

A	tube area, [m^2]
A_1	constant given in Table 4
a	dimensionless tube spacing parameter
b	dimensionless tube spacing parameter
C_1	tube fluid heat capacity rate, [W/K]
C_2	shell fluid heat capacity rate, [W/K]
C_n	constant based on number of rows
C_p	specific heat, [J/(kg K)]
D	tube inside diameter, [m], $D = 2 \times r_{in}$
f	friction factor
h	heat transfer coefficient for each fluid, [W/(m^2 K)]
$\bar{h}_{hx}$	overall heat transfer coefficient, [W/(m^2 K)]
k	thermal conductivity, [W/(m K)]
L	tube length, [m]

L_e	hydraulic entrance length, [m]
m_1	constant given in Table 4
$\dot{m}$	mass flow rate, [kg/s]
n_1	constant given in Table 4
N_{seg}	number of segments
N_r	number of rows
N_t	number of tubes in each row
N_s	number of stacks
NTU	number of heat transfer units
Nu	Nusselt number
Pr	Prandtl number
q	heat load, [W]
Re_D	Reynolds number based on tube diameter
U	overall heat transfer coefficient of the heat exchanger, [W/(m^2 K)]

Greek

ν	kinematic viscosity, [m^2/s]

subscripts

1	tube side fluid
2	shell side fluid
in	inlet
m	metal
out	outlet
w	wall

1. Introduction

Shell and tube heat exchangers are commonly used in many capacities for heating and cooling, and their design has been an important research topic for many years. In the past, the design and performance of shell and tube heat exchangers has been extensively studied [3–15]. However, with recent advancements in additive manufacturing, through which "unconventional" designs can be investigated, there has been an increased interest in improving the effectiveness and efficiency of traditional heat exchangers while driving down the manufacturing and operational costs. As such, design tools that are both efficient and accurate are needed to investigate many possible configurations/geometries in a wide design space.

The concept of multi-scale heat exchanger design was previously studied by Bejan et al. [16–21], Zimparov et al. [22], da Silva et al. [23], Chen et al. [24], and Lorenzini et al. [25]. A new design for shell and tube heat exchangers based on constructal law [26] was recently proposed by Sabau et al. [1, 2]. Their heat exchanger design incorporated the multi-scale design with successive plenums at several length-scale levels to attain better thermal performance with limited cost increases. The original configuration was in a cross-flow configuration where the working fluid, in this case brine, was inside the tubes and the refrigerant (R134A) flowed on the outside or the shell side of the heat exchanger. Sabau et al. [1, 2] demonstrated that their concept had lower overall cost and better thermal performance when compared to a traditional shell and tube heat exchanger with the same heat load requirements.

As indicated earlier, it is always desirable to lower the overall cost of a

heat exchanger while keeping the thermal performance unaffected or even improved. One possible way of achieving this goal is reversing the flow direction of one the fluids. According to Incropera et al. [27], for the same inlet and outlet conditions the log mean temperature difference for counter flow exchangers exceeds that of the parallel flow. Assuming the same value of the overall heat transfer coefficient for both flows, the counter flow heat exchanger requires less surface area to attain the same heat transfer rate as the parallel flow. The same holds true for the cross-flow and counter cross-flow configurations.

The overall goal here is to rely on the new concept [1, 2] and investigate configurations that lower the cost per heat load while improving the thermal performance. Using the computational methodology presented in this paper, the thermal performance of different heat exchanger configurations in counter cross-flow are studied. These results are then compared to the ones presented by [1, 2] to determine the effects of the flow direction on the thermal performance and overall cost. As will be demonstrated later in this paper, the counter cross-flow setup provides higher heat loads for the same geometry configurations as the cross-flow heat exchanger.

2. Design Variables

Figure 1 shows a sample heat exchanger design from Sabau et al. [1, 2]. This design consists of three flow levels where the smallest scale is the flow inside the cylindrical tubes. To enhance the thermal performance of the heat exchanger, the tube lengths are set to be equal to the their hydraulic entrance length [17, 26]. For turbulent flows, the thermal and hydraulic entrance are

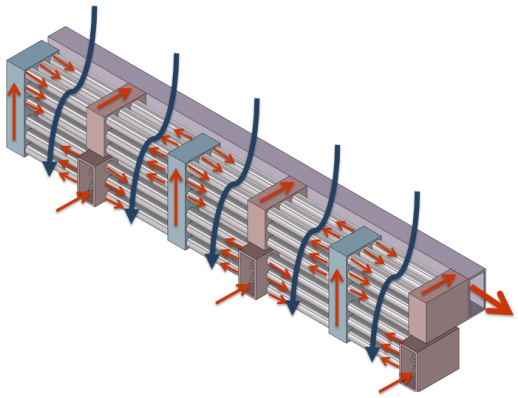

Figure 1: A sample heat exchanger design from [1, 2] in counter cross-flow, showing the flow direction of brine and refrigerant with inlet level 1 removed for clarity.

approximately the same, and therefore, can be used interchangeably.

The entrance length idea was first introduced by Bejan [17] for the design of dendritic heat exchangers. At the entrance length region of the tubes, the Nusselt number is much higher which translates into higher heat transfer coefficients. Sizing the tubes to their hydraulic (thermal) entrance length maximizes the thermal performance of the heat exchanger while keeping the material cost low, which in turn reduces the cost per heat load metric for the heat exchanger. For each individual heat exchanger configuration, the tube lengths at level 3 are calculated according to Zhi-Qing [28] using Eq. (1) to match the turbulent hydraulic entrance length of the brine flowing inside.

$$L_e = 1.36\ D\ \mathrm{Re}_D^{1/4} \tag{1}$$

At each flow level, the heat exchanger is made up of tubes or ducts of varying sizes as shown in Fig. 1. At the smallest length scale, the number of tubes can vary horizontally (n_3), or vertically (ns_3). In a similar fashion,

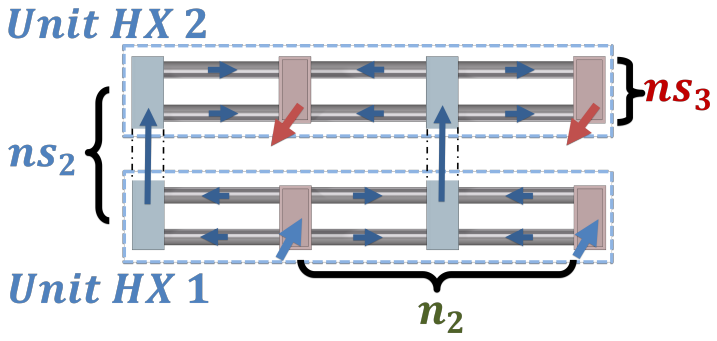

(a)

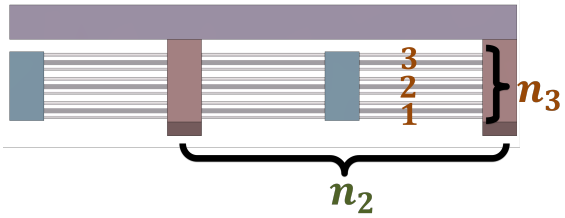

(b)

Figure 2: Sample of heat exchanger design from [1, 2] showing all four geometry-based design variables. (a) Sectioned front view with level 1 removed for clarity showing two unit heat exchangers. Arrows represent the brine flow direction. (b) Top view of the heat exchanger showing the level 2 channels arrangements.

at level 2 scale (the ducts connected at each end of the tubes), the number of inlet ducts can vary horizontally (n_2) and vertically (ns_2). This is also shown in Figs. 2a and 2b. For the heat exchanger depicted here the number of ducts and tubes are taken to be $n_3 = 3$, $ns_3 = 2$, $n_2 = 2$ and $ns_2 = 2$. Different combinations of n_3, ns_3, n_2 and ns_2 should be considered to find the best performing heat exchanger design, and to examine the overall effects of the number of stacks on the heat exchanger performance.

In essence, this new heat exchanger design consists of multiple "unit" heat exchangers that are assembled in parallel to create a multi-stack heat exchanger as shown in Fig. 2a. The number of level 2 channels in each of the "unit" heat exchangers is equal to $2n_2 - 1$, where the design variable n_2 is the number of inlets for the brine. In other words, it is the number of times the total brine mass flow rate is evenly distributed in level 2. The level 2 channels in turn evenly distribute the brine to level 3 tubes. The total number of tubes in a row, as seen by the refrigerant as it enters the space between 2 adjacent level 2 channels, corresponds to the design variable n_3. That is, there are n_3 number of tubes in a row connecting two adjacent level 2 channels, where one channel is the inlet channel for the tubes in that row and the other is the exit channel. Therefore, in the unit heat exchanger, there are a total of $n_3 \times (2n_2 - 1)$ tubes immediately facing the refrigerant as it enters the system. This is the core architecture of the heat exchanger where the outside fluid passes over a single wall of round tubes and then exits the system.

Additionally, this configuration can be expanded by introducing a new design variable and adding more tubes behind the first row of tubes in a

staggered arrangement and extending the width of the level 2 channel to accommodate these new rows of tubes. The total number of parallel rows of tubes in the unit heat exchanger is represented by the design variable ns_3. These additional rows of tubes are connected to the same level 2 channels as the first row, and therefore, share the same inlet temperature for the brine as the first row in front of them.

To further enhance the performance of the heat exchanger, additional unit heat exchanger configurations can be connected in parallel to the first unit to create a stacked heat exchanger. The total number of stacked unit heat exchangers is represented by ns_2. It is assumed that both the inside and the outside fluids are well mixed as they exit each unit heat exchanger, and thus, the average brine and refrigerant exit temperatures of the first unit heat exchanger are used as the inlet temperatures for the 2nd unit and so on.

The tube side fluid enters the heat exchanger at level 1, where it is divided evenly between the level 2 inlets such that $\dot{m}_{L1} = \dot{m}_{L2} \times n_2$. The tube side fluid is also assumed to be evenly distributed between the level 3 tubes attached to the first stack ($ns_2 = 1$) such that $\dot{m}_{L1} = \dot{m}_{L3} \times (2n_2 - 1) \times n_3 \times ns_3$.

The effect of tube spacing is also considered in the overall cost and thermal performance of the design. Figure 3 shows the two variables a and b that are adjusted to attain the best tube spacing for this heat exchanger design.

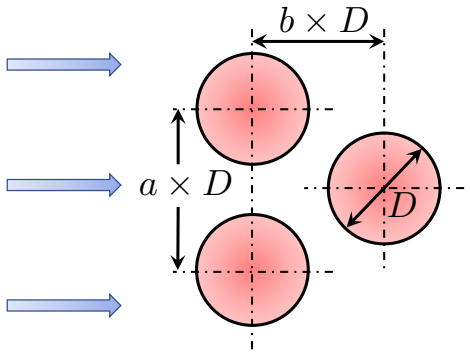

Figure 3: Definition of dimensionless spacing parameters a and b for a staggered bank of tubes in level 3.

3. Thermal Performance Analysis of New Counter Cross-flow Heat Exchangers

In this work, two separate models were developed for the performance analysis of the cross-flow and counter cross-flow heat exchanger design. The first model, as presented and discussed in this section, is used to gauge the thermal performance of the new design cross-flow and counter cross-flow heat exchangers using the entrance length concept. The second model that was developed, is used to study thermal performance characteristics of a traditional shell and tube heat exchanger. The traditional shell and tube design is used as a baseline design in order to compare its performance with the new entrance length cross-flow and counter cross-flow heat exchanger design concept allowing us to assess the advantages and disadvantages of the new approach. For brevity, the theory behind the shell and tube heat exchanger design will not be presented in this work. However, detailed information and discussion can be found in an earlier publication by Sabau et al. [2].

The entrance-length concept presented here is approached numerically

by calculating outlet temperatures for the mixed-unmixed counter cross-flow heat exchangers. Unlike previous studies reported in the literature, only inputs for the current approach are the material properties, inlet temperatures, mass flow rates for each stream, and the geometric variables such as tube diameter and tube thickness.

At its core, this method computes the temperature distribution along each tube based on the energy balance between the shell side fluid and the tube side fluid. An initial guess is made for the outlet temperature and the heat transfer coefficient, and their values are updated iteratively based on the energy balance in the system. It should be noted that, the method is generalized and can be used to model any configuration with varying number of tubes, tube diameters, and tube spacing. The analysis assumes that the flow is turbulent and that the fluid is fully mixed inside the tubes and unmixed on the shell side, except between each stack, where mixing occurs. It also assumes that the working fluids are evenly distributed through each tube as well as outside of each tube. Due to the periodicity, a simplified version of each configuration can be used to calculate the temperature distribution.

Each tube is divided into N_{seg} number of segments, that results in $N_{seg}+1$ nodes along the tube for the tube side fluid and N_{seg} nodes on the outside of the tube for the shell fluid. Therefore, the temperature matrix for the tube side fluid has dimensions of $(N_{seg}+1) \times N_t$ and the outside fluid temperature matrix has dimensions of $N_{seg} \times (N_t + 1)$ where N_t is the total number of tubes in each row. In what follows, the upper-case T will represent the tube side fluid nodes and the lower-case t will represent the shell side fluid. The index i increases along the length of the tube from top to bottom, and the

index j increases from left to right, where each j represents a tube.

A representative computational grid for two adjacent tubes in counter cross-flow configurations is depicted in Fig. 4, where the arrows show the direction of the flow. As can be seen, the two nodes, namely $(i, j+2)$ and $(i+1, j+2)$, correspond to the inlets for the shell side fluid, and therefore, their temperatures $[t(i, j+2)$ and $t(i+1, j+2)]$ are known. This means that the inlet temperature boundary condition $(j = j_{max})$ imposed on the shell side fluid is on the right side of the temperature matrix. In contrast, for a cross-flow heat exchanger the temperature boundary is on the left side of the matrix or when $j = 1$. This technique assumes that the tube side fluid always flows from top to bottom in all tubes. To mimic the serpentine configuration of the heat exchanger, an average temperature condition is imposed on the solution for the outside temperature nodes at the exit of each stack before starting the next iteration. Therefore, according to Fig. 4 and assuming a single tube per stack, $T(i+2, j) = T(i, j+1)$. Furthermore, due to averaging, $t(i, j+2) = t(i+1, j+2)$ and so on.

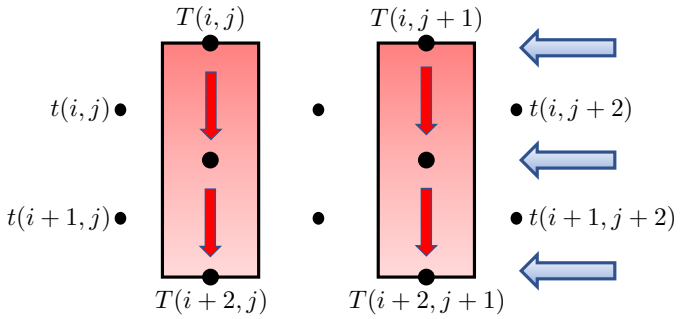

Figure 4: Grid point locations for the shell side (t) and tube side (T) temperature nodes. (counter cross-flow)

The mass flow rate, $\dot{m}_2$, is calculated based on the assumption that the total

flow rate is evenly distributed to N_t tubes. Using conservation of energy, the unknown temperature values, (i.e., $T(i+1,j)$ and $t(i,j+1)$) can be written in terms of the known temperatures in the adjacent nodes. That is,

$$\frac{\dot{m}_2}{N_t N_{seg}} C_{p2} \left[t\left(i,j+1\right) - t\left(i,j\right) \right] = \frac{\dot{m}_1}{N_t N_r} C_{p1} \left[T\left(i,j\right) - T\left(i+1,j\right) \right] \tag{2}$$

Furthermore, the temperature values at each node can be related to the overall heat transfer coefficient, $\bar{h}_{hx}$, through

$$\frac{t\left(i,j\right) + t\left(i,j+1\right)}{2} - T\left(i+1,j\right) = \left[\frac{t\left(i,j\right) + t\left(i,j+1\right)}{2} - T\left(i,j\right) \right] \exp\left(-\beta\right) \tag{3}$$

where

$$\beta = \frac{2\pi r_{out} \bar{h}_{hx} L}{C_1 N_{seg}} \tag{4}$$

Here $\bar{h}_{hx}$ depends on both inside and outside heat transfer coefficients which are calculated based on Nusselt number correlations. The definition of $\bar{h}_{hx}$ used in Eq. (4) and other relevant relationships are provided in Appendix A. Additionally, the tube length L is taken to be the thermal entrance length of the brine, which is calculated individually for each heat exchanger configuration through Eq. (1).

The idea behind the entrance length concept was first introduced by Bejan [17] to further improve the thermal performance of dendritic heat exchanger design. This enhanced heat transfer performance is due to higher heat transfer coefficients in the entrance region of the channel or the tube. For a round tube, the local Nusselt number has much higher values in the entrance region of the tube. The Nusselt number sharply drops as the flow develops approaching a constant value for the fully developed region. These local Nusselt number values for the tube side fluid can be calculated using

Eq. (12), which in turn depends on the tube friction factor given by Eq. (13). The value of the local Nusselt number directly controls the local heat transfer coefficient, and hence, the overall thermal performance of the heat exchanger. In other words, the tube side fluid's heat transfer coefficient in the entrance region of the tubes is much higher when the flow is developing.

Therefore, to take advantage of the higher heat transfer coefficients, the tubes are designed to have lengths equal to the thermal entrance length of the fluid flowing inside, Eq. (1). This length depends on the particular fluid's properties at a given temperature, as well as the fluid's mass flow rate. In this approach, the entrance length is calculated separately for each individual heat exchanger configuration. It is also possible to combine different flow levels and different tube diameters, each with their own entrance length and flow characteristics. For the shell fluid flowing through a bank of tubes, the average Nusselt number is calculated using Eq. (14).

Next, it is assumed that the surface temperature for each segment of the tube is constant and equal to the average of the outside temperatures between the nodes j and $j+1$. Rearranging Eqs.(2) and (3) one gets:

$$t\left(i,j+1\right)-\left[\frac{\dot{m}_1}{\dot{m}_2}\frac{N_{seg}}{N_r}\frac{C_{p1}}{C_{p2}}\right]T\left(i+1,j\right)=\left[\frac{\dot{m}_1}{\dot{m}_2}\frac{N_{seg}}{N_r}\frac{C_{p1}}{C_{p2}}\right]T\left(i,j\right)+t\left(i,j\right) \quad (5)$$

and

$$T\left(i+1,j\right)-\left[1+\exp\left(-\beta\right)\right]t\left(i,j+1\right)=t\left(i,j\right)-\exp\left(-\beta\right)\left[T\left(i,j\right)-t\left(i,j\right)\right] \quad (6)$$

Note that Eqs. (5) and (6) can be written as a linear system as:

$$\begin{bmatrix} M & 1 \\ \\ 1 & E \end{bmatrix} \begin{Bmatrix} T(i+1,j) \\ \\ t(i,j+1) \end{Bmatrix} = \begin{Bmatrix} T(i,j)M + t(i,j) \\ \\ T(i,j)\,(2E+1) - t(i,j)E \end{Bmatrix} \tag{7}$$

where M and E are constant values for each segment of the tube and are defined as:

$$E = 0.5\left[\exp\left(-\beta\right) - 1\right] \tag{8}$$

$$M = \frac{\dot{m}_1}{\dot{m}_2}\frac{N_{seg}}{N_r}\frac{C_{p1}}{C_{p2}} \tag{9}$$

For the entire heat exchanger, Eq. (7) is evaluated at every node and the governing equation turns into a block diagonal system of equations in the form of $\mathbf{Ax} = \mathbf{b}$ where $\mathbf{A}$ is a square matrix of size $n \times n$ and $\mathbf{b}$ is a column vector of length n, where $n = N_s \times N_r \times N_{seg}$.

The system of equations for the entire heat exchanger is solved iteratively, until convergence - based on the outlet temperature residuals (0.01 ^{o}C) and the overall energy balance error (less than 0.1%) of the system. Preliminary simulations indicate that the overall number of iterations needed to reach convergence depends on the size of the solution matrix ($n \times n$) as well as the maximum allowable error in the solution. However, in all cases considered, the total computational time to attain convergence was on the order of minutes on a modern desktop system.

The computational method was verified by modeling heat exchanger configurations used by Shah and Pignotti [12]. Although not presented here, the results closely matched those presented in Ref. [12], with an error of less than 1.05% [2] for all configurations.

4. Results

The thermal performance results for the new counter cross-flow heat exchanger designs are presented in this section and compared to cross-flow heat exchanger results published previously by Sabau et al. [1, 2].

To investigate the effects of counter cross-flow on the thermal performance of the new heat exchangers design, five a/b tube arrangements were chosen, while keeping other design variables constant. For different values of a/b, the NTU, overall cost and the cost per heat load are calculated. The total cost (in US dollars) is calculated using Eq. (17) given in Appendix B [29], assuming a total of $8,760$ hours of operation per year.

For the results in Fig. 5 the design constants are, $n_2 = 4$, $ns_2 = 8$, $n_3 = 25$, $ns_3 = 4$. Figure 5 shows the total cost of the cross-flow (CF) and the counter cross-flow (CCF) heat exchanger (HX) for five different tube arrangements, a/b, with $a = 2$. For both CF and CCF configurations, as the value of a/b increases from 1.5 to 3.5, the overall cost decreases and the NTU increases.

Comparing Figs. 5a and 5b at each value of a/b tube arrangement, it is clear that for both CF and CCF configurations, the overall cost of the heat exchangers are about the same. However, the CCF HX has higher NTU compared to its corresponding CF counterpart, which indicates the CCF configuration has better thermal performance than CF for all tube arrangements considered.

The calculated NTU values, at each a/b tube arrangement, for both cross-flow and counter cross-flow HXs are shown in Table 1. The percent increase in NTU from CF to CCF is between 5 to 16 percent depending on the a/b tube arrangement. It is clear that the larger a/b values result in higher NTU

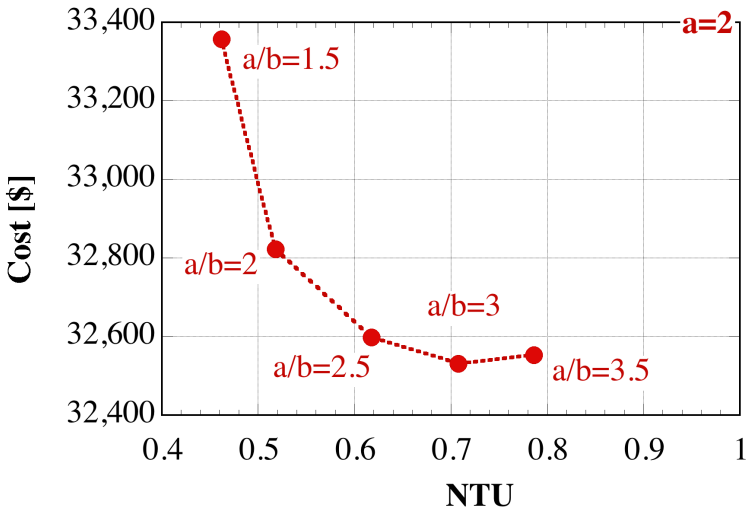

(a)

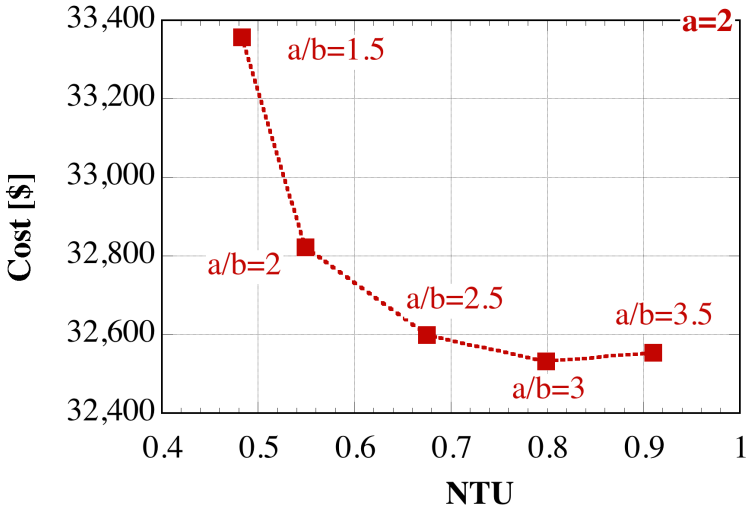

(b)

Figure 5: NTU vs. overall cost [$] (a) Cross-flow heat exchanger (b) Counter cross-flow heat exchanger

Table 1: Cross-flow and counter cross-flow NTU comparison.

a/b	NTU		%diff
	Cross-Flow	Counter Cross-Flow	
1.5	0.46	0.48	4.6
2.0	0.52	0.55	6.0
2.5	0.62	0.68	9.4
3.0	0.71	0.80	12.9
3.5	0.79	0.91	15.8

increase when going from the CF to CCF configuration.

Next, Fig. 6 shows the cost per heat load [$/kW] vs NTU for both CF and CCF HX configurations. As expected, the CCF HX has better thermal performance compared to the CF setup. For each tube arrangement shown in Fig. 6, the CCF HX has higher NTU and lower cost per heat load. Since the overall cost for both heat exchangers are about the same, the lower cost per heat load for the CCF HX also indicates that higher heat loads are obtained for each a/b arrangement.

Table 2 shows the comparison between cost per heat load [$/kW] for the CF and CCF configurations. As can be seen, the overall cost per heat load [$/kW] decreases with increasing a/b for both CF and CCF configurations. Additionally, for each value of a/b, the counter cross-flow HX has lower cost per heat load [$/kW] compared to the cross-flow HX, which depending on the value of a/b is between 3.2 to 8.7 percent. For the CCF HX the most cost effective tube arrangement with the best thermal performance is $a/b = 3.5$. This was also chosen by Sabau et al. [2] as the best performing

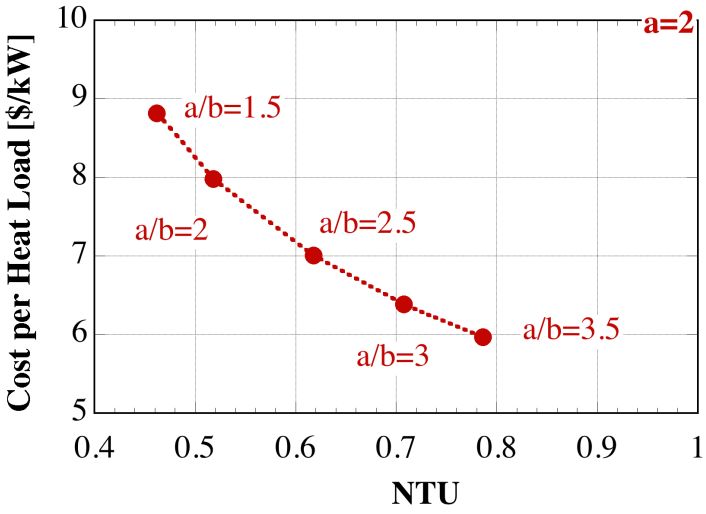

(a)

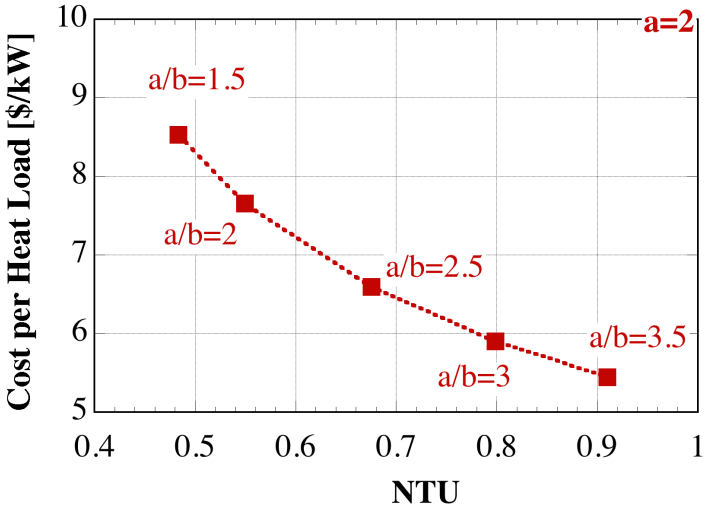

(b)

Figure 6: Cost per heat load [$/kW]. (a) cross-flow. (b) counter cross-flow.

Table 2: Cross-flow and counter cross-flow cost per heat load [$/kW] comparison.

a/b	Cost per heat load [$/kW]		%diff
	Cross-Flow	Counter Cross-Flow	
1.5	8.82	8.53	3.2
2.0	7.98	7.65	4.1
2.5	7.01	6.60	5.9
3.0	6.38	5.90	7.5
3.5	5.96	5.44	8.7

tube arrangement for the cross-flow configuration.

Next, additional configurations were considered for $a/b = 3.5$ in order to assess the performance based on the number of stacks in level two, ns_2. A set of values for ns_2 between 4 and 16 were chosen, while keeping $n_2 = 4$ constant and varying n_3 as well as ns_3 such that $(2n_2 - 1) \times n_3 \times ns_3 \approx 700$.

Figs 7 and 8 show the cost and cost per heat load for for the counter cross-flow heat exchanger. The filled symbols in Fig. 7 represent the cases with heat loads in the range of 4.5 MW $\leqslant q \leqslant$ 5.5 MW, while the filled in points in Fig. 8 show the cases where the heat loads are over 5.5 MW. Depending on the tube arrangement and the HX configuration, it is possible to achieve heat loads greater, equal to or less than 5 MW with $ns_2 = 6$, while $ns_2 \geqslant 8$ will produce heat loads that are greater than 5 MW.

Table 3 shows the performance data for both CF and CCF HX for $n_2 =$ 4 and 12, $ns_2 = 4$ and 8, while varying n_3 and ns_3 to keep the total number of tubes in one stack approximately constant $[(2n_2 - 1) \times n_3 \times ns_3 \approx 700]$.

The maximum increase in the heat load was about 17% going from the

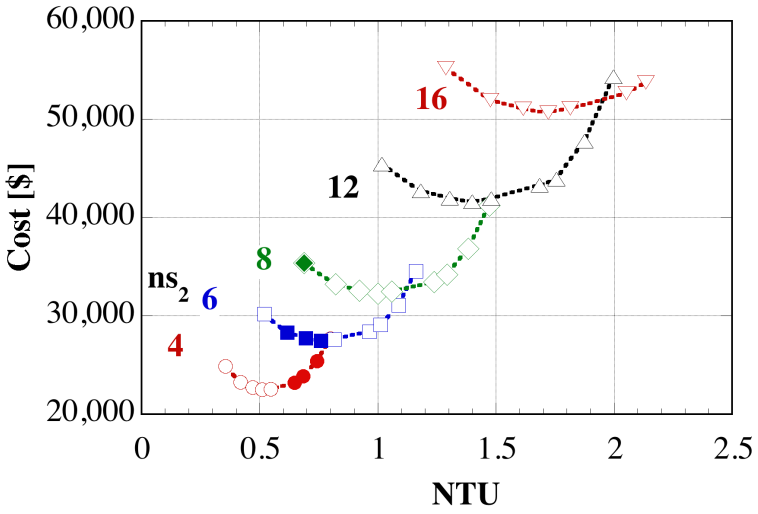

(a)

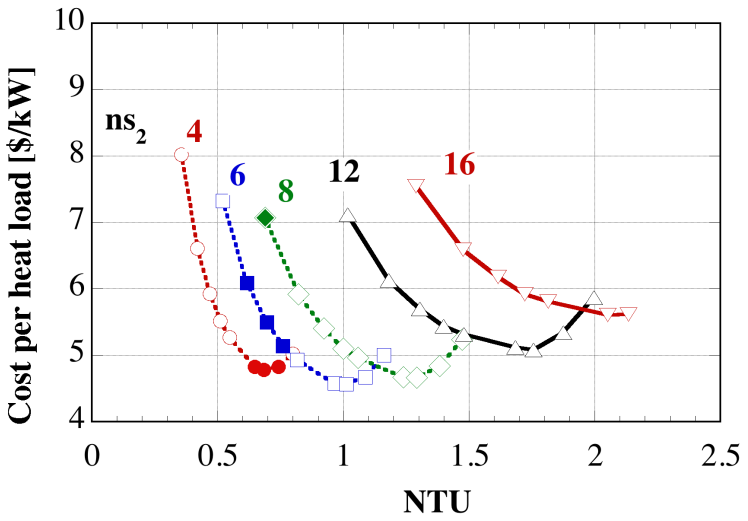

(b)

Figure 7: Calculated (a) Cost [$] and (b) Cost per heat load [$/kW] as a function of NTU for varying ns_2. Filled in points represent configurations with heat loads in the range of 4.5 MW $\leqslant q \leqslant$ 5.5 MW.

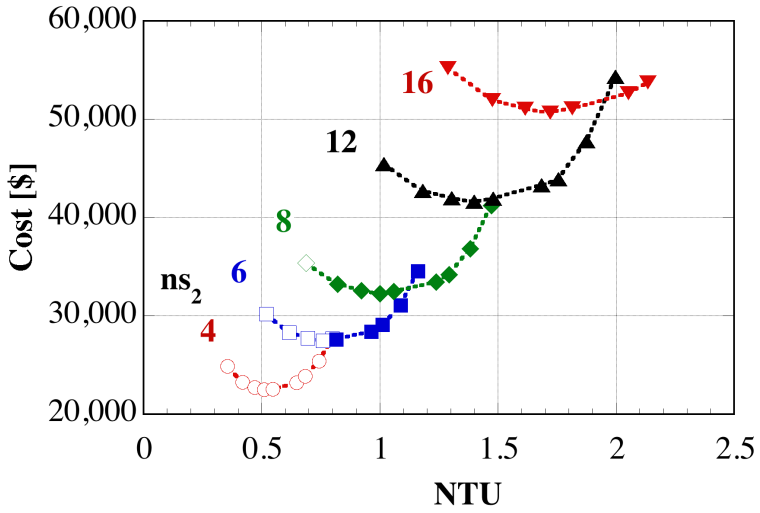

(a)

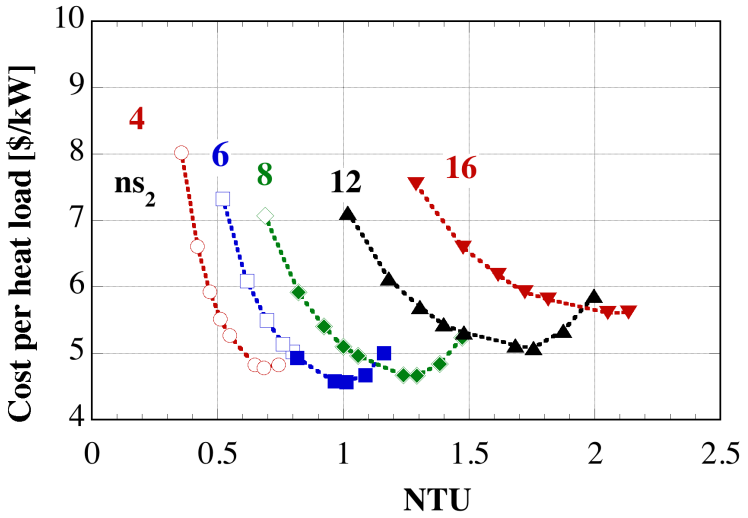

(b)

Figure 8: Calculated (a) Cost [$] and (b) Cost per heat load [$/kW] as a function of NTU for varying ns_2. Filled in points represent configurations with heat loads over 5.5 MW.

Table 3: Performance comparison between Cross-Flow vs. Counter Cross-Flow configurations. $[(2n_2 - 1) \times n_3 \times ns_3 \approx 700]$

n_2	ns_2	n_3	ns_3	q [MW]		%diff	NTU		%diff	Cost/q [$/kW]		%diff
				CF	CCF		CF	CCF		CF	CCF	
4	4	33	3	3.4	3.5	2.3	0.40	0.42	3.1	6.79	6.64	2.3
		25	4	3.7	3.8	2.7	0.45	0.46	3.5	6.17	6.00	2.6
		20	5	3.9	4.0	3.4	0.48	0.50	4.6	5.79	5.60	3.2
		17	6	4.1	4.2	4.2	0.51	0.54	5.7	5.56	5.34	4.0
		10	10	4.5	4.7	6.0	0.58	0.64	9.0	5.18	4.89	5.7
		8	12	4.6	4.9	6.7	0.61	0.67	10.0	5.18	4.86	6.3
		7	15	4.8	5.2	7.5	0.65	0.72	11.5	5.27	4.91	6.9
		5	20	5.0	5.4	8.4	0.69	0.78	12.9	5.53	5.10	7.7
	8	33	3	5.1	5.6	8.9	0.72	0.82	14.0	6.46	5.93	8.2
		25	4	5.5	6.0	9.5	0.79	0.91	15.6	5.96	5.44	8.7
		20	5	5.7	6.3	10.4	0.84	0.98	17.7	5.68	5.14	9.4
		17	6	5.9	6.5	11.5	0.88	1.05	19.8	5.55	4.98	10.3
		10	10	6.2	7.1	13.8	0.97	1.21	25.2	5.37	4.72	12.1
		8	12	6.3	7.3	14.7	1.00	1.27	27.1	5.38	4.71	12.4
		7	15	6.5	7.5	16.1	1.04	1.35	30.1	5.65	4.91	13.2
		5	20	6.6	7.7	17.5	1.07	1.43	33.3	6.24	5.32	14.7
12	4	17	2	3.1	3.2	0.3	0.36	0.36	0.5	9.31	9.28	0.3
		11	3	3.5	3.6	2.0	0.42	0.43	2.8	7.72	7.57	2.0
		8	4	3.8	3.9	2.7	0.46	0.47	3.8	6.96	6.78	2.6
		7	5	4.0	4.1	3.8	0.50	0.52	5.1	6.52	6.29	3.6
		5	6	4.1	4.3	4.1	0.52	0.55	6.0	6.30	6.05	4.0
		3	10	4.6	4.9	6.6	0.60	0.66	9.6	6.11	5.74	6.2
		3	12	4.8	5.1	7.3	0.64	0.71	11.1	6.04	5.63	6.8
		2	15	4.9	5.3	7.9	0.67	0.76	12.4	6.70	6.21	7.3
	8	17	2	4.8	5.1	6.3	0.64	0.70	9.6	8.40	7.90	5.9
		11	3	5.2	5.7	9.2	0.74	0.84	14.7	7.15	6.55	8.4
		8	4	5.5	6.1	9.8	0.80	0.93	16.3	6.53	5.95	8.9
		7	5	5.8	6.4	10.9	0.86	1.02	18.6	6.33	5.70	9.8
		5	6	5.9	6.6	11.9	0.89	1.07	20.3	6.01	5.38	10.6
		3	10	6.3	7.2	14.5	0.99	1.25	26.6	6.07	5.31	12.6
		3	12	6.4	7.5	15.8	1.03	1.33	29.7	6.27	5.44	13.3
		2	15	6.5	7.7	17.0	1.06	1.40	32.2	7.05	6.03	14.4

CF to CCF configuration. This percent increase is seen for both $n_2 = 4$ and 12 for $ns_2 = 8$. The configurations with the largest increase in the heat load also represent the largest decrease in cost per heat load. The lowest cost per heat load is achieved with $n_2 = 4$, $ns_2 = 3$, $n_3 = 8$ and $ns_3 = 12$ in the CCF configuration. This configuration has a cost per heat load of 4.71 [$/kW].

Having investigated the advantages of the CCF configuration over the CF one, we now turn our attention to the performance of the entrance-length design concept compared to traditional shell and tube designs. Figure 9 presents such a comparison for varying heat loads. For the new design, values of $n_2 = 4$ and $ns_2 = 4$ are used, and n_3 and ns_3 are varied as shown in Table 3. For the shell and tube heat exchanger, each data point represents the lowest calculated cost per heat load configuration for the given heat load, where the heat load increases from 3.5 MW to 6.5 MW. As seen in this figure, the counter cross-flow configuration has lower cost per heat load compared to both cross-flow with the same design variables as well as the traditional shell and tube heat exchanger design. As such, the current concept is significantly better than the current state of the art.

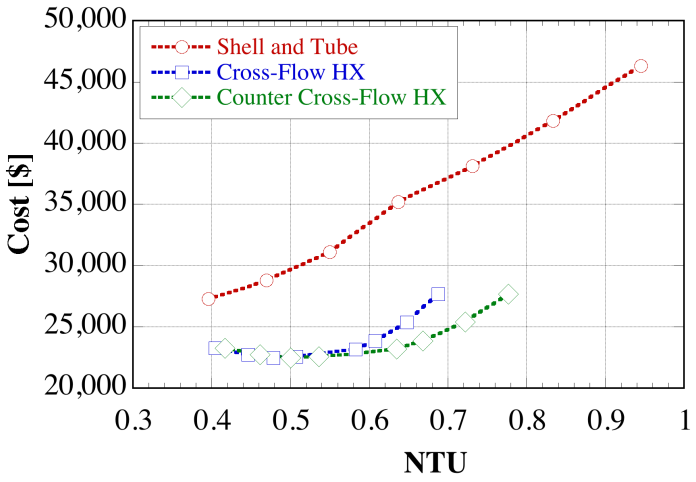

(a)

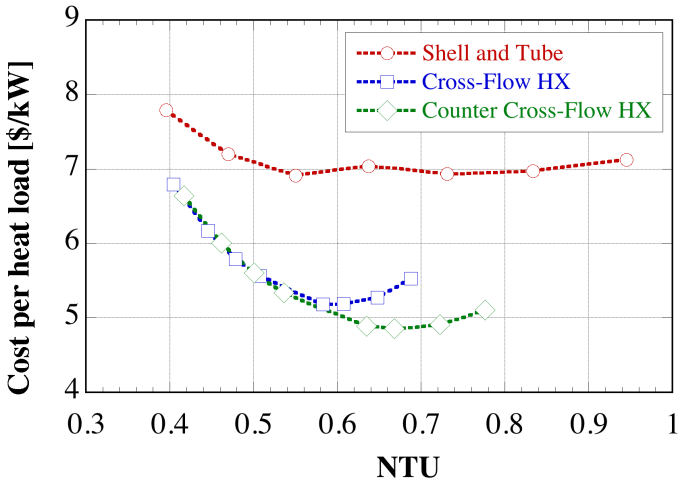

(b)

Figure 9: Comparison between the new design Cross-Flow, Counter Cross-Flow and traditional shell and tube heat exchangers with heat loads of 3.5 MW $\leqslant q \leqslant$ 6.5 MW. a) cost[$]. (b) cost per heat load [$/kW]

5. Conclusions

The objective of this study was to improve the thermal performance and lower the overall cost of a newly introduced cross-flow heat exchanger design, by changing the configuration to counter cross-flow. By using a numerical approach to solve for the temperature distribution in the heat exchanger it was possible to determine the thermal performance and overall cost of the cross-flow configuration. Results indicated that using the same design variables as the cross-flow counterpart, it was possible to improve the thermal performance of the new design by as much as 17% and lower the total cost by as much as 14%. In geothermal applications the total available energy depends on the hydro-thermal resources. This limits the heat exchanger's maximum attainable heat load. For this reason it is not possible to improve the thermal performance of the heat exchanger any further. However, it is possible to build a smaller scale heat exchanger in counter cross-flow to match the same heat load levels as the cross-flow heat exchanger but at a lower overall cost.

Acknowledgment

This work was performed for the project "Freeform Heat Exchangers for Binary Geothermal Power Plants" sponsored by the Geothermal Technologies Program, Office of Energy Efficiency and Renewable Energy, U.S. Department of Energy under contract DE-AC05-00OR22725, Oak Ridge National Laboratory, managed and operated by UT-Battelle, LLC. The authors greatly appreciate the support provided.

References

[1] A. S. Sabau, A. H. Nejad, J. W. Klett, A. Bejan, K. Ekici, Novel evaporator geometries based on entrance-length flow-paths for geothermal binary power plants, in: Proceedings of the ASME 2016 International Mechanical Engineering Congress and Exposition, no. IMECE2016-67660, ASME, 2016.

[2] A. S. Sabau, A. H. Nejad, J. W. Klett, A. Bejan, K. Ekici, Novel evaporator architecture with entrance-length crossflow-paths for supercritical organic rankine cycles, International Journal of Heat and Mass Transfer 119 (2018) 208–222.

[3] L. D. Ruiz, C. A. Peñaloza, G. V. Ochoa, Effect of the mass flow rate on the heat transfer phenomena in a shell and tube heat exchanger, International Journal of Applied Engineering Research 13 (14) (2018) 11387–11391.

[4] Y. Yin, D. Zhu, J. Sun, X. Li, J. Zhang, C. Lin, Comparison of a novel un-baffled and a conventional shell-and-tube dry-expansion evaporator, Applied Thermal Engineering 113 (2017) 1137–1145.

[5] A. Alimoradi, F. Veysi, Prediction of heat transfer coefficients of shell and coiled tube heat exchangers using numerical method and experimental validation, International Journal of Thermal Sciences 107 (2016) 196–208.

[6] M. K. Rathod, J. Banerjee, Thermal performance enhancement of shell

and tube latent heat storage unit using longitudinal fins, Applied Thermal Engineering 75 (2015) 1084–1092.

[7] J. Wen, H. Yang, S. Wang, Y. Xue, X. Tong, Experimental investigation on performance comparison for shell-and-tube heat exchangers with different baffles, International Journal of Heat and Mass Transfer 84 (2015) 990–997.

[8] L. Cabezas-Gomez, M. J. Saiz-Jabardo, H. A. Navarro, P. E. L. Barbieri, New thermal effectiveness data and formulae for some cross-flow arrangements of practical interest, International Journal of Heat and Mass Transfer 69 (2014) 237–246.

[9] J. Navarro-Esbrí, F. Molés, B. Peris, Á. Barragán-Cervera, J. M. Mendoza-Miranda, A. Mota-Babiloni, J. M. Belman, Shell-and-tube evaporator model performance with different two-phase flow heat transfer correlations. Experimental analysis using R134a and R1234yf, Applied Thermal Engineering 62 (1) (2014) 80–89.

[10] L. Cabezas-Gomez, H. A. Navarro, M. J. Saiz-Jabardo, Thermal performance of multipass parallel and counter-cross-flow heat exchangers, ASME Journal of Heat Transfer 129 (3) (2006) 282–290.

[11] H. A. Navarro, L. Cabezas-Gomez, A new approach for thermal performance calculation of cross-flow heat exchangers, International Journal of Heat and Mass Transfer 48 (18) (2005) 3080–3088.

[12] R. K. Shah, A. A. Pignotti, Thermal analysis of complex crossflow ex-

changers in terms of standard configurations, ASME Journal of Heat Transfer 115 (2) (1993) 353–359.

[13] A. A. Pignotti, G. O. Cordero, Mean temperature difference in multipass crossflow, ASME Journal of Heat Transfer 105 (3) (1983) 584–591.

[14] D. P. Sekulič, R. K. Shah, A. A. Pignotti, A review of solution methods for determining effectiveness-NTU relationships for heat exchangers with complex flow arrangements, Applied Mechanics Reviews 52 (3) (1999) 97–117.

[15] A. A. Pignotti, R. K. Shah, Effectiveness-number of heat transfer units relationships for heat exchanger complex flow arrangements,, International Journal of Heat and Mass Transfer 35 (5) (1992) 1275–1291.

[16] A. Bejan, M. Alalaimi, A. Sabau, S. Lorente, Entrance-length dendritic plate heat exchangers, International Journal of Heat and Mass Transfer 114 (2017) 1350–1356.

[17] A. Bejan, Dendritic Constructal heat exchanger with small-scale crossflows and larger-scale counterflows, International Journal of Heat and Mass Transfer 45 (23) (2002) 4607–4620.

[18] A. Bejan, M. R. Errera, Convective trees of fluid channels for volumetric cooling, International Journal of Heat and Mass Transfer 43 (17) (2000) 3105–3118.

[19] A. Bejan, From heat transfer principles to shape and structure in nature: Constructal theory, Journal of Heat Transfer 122 (3) (2000) 430–449.

[20] A. Bejan, Shape and Structure, from Engineering to Nature, Cambridge University Press, 2000.

[21] A. Bejan, S. Lorente, The Constructal law and the thermodynamics of flow systems with configuration, International Journal of Heat and Mass Transfer 47 (14-16) (2004) 3203–3214.

[22] V. Zimparov, A. Da Silva, A. Bejan, Constructal tree-shaped parallel flow heat exchangers, International Journal of Heat and Mass Transfer 49 (23-24) (2006) 4558–4566.

[23] A. K. da Silva, S. Lorente, A. Bejan, Constructal multi-scale tree-shaped heat exchangers, Journal of Applied Physics 96 (3) (2004) 1709–1718.

[24] L. Chen, H. Feng, Z. Xie, F. Sun, Thermal efficiency maximization for H-and X-shaped heat exchangers based on Constructal theory, Applied Thermal Engineering 91 (2015) 456–462.

[25] G. Lorenzini, C. Biserni, L. Rocha, Geometric optimization of X-shaped cavities and pathways according to Bejan's theory: comparative analysis, International Journal of Heat and Mass Transfer 73 (2014) 1–8.

[26] A. Bejan, S. Lorente, Design with Constructal Theory, Wiley, Hoboken, NJ, 2008.

[27] F. P. Incropera, D. P. DeWitt, T. L. Bergman, A. S. Lavine, Fundamentals of Heat and Mass Transfer, 6th Edition, Wiley, Hoboken, NJ, 2011.

[28] W. Zhi-qing, Study on correction coefficients of laminar and turbulent entrance region effect in round pipe, Applied Mathematics and Mechanics 3 (3) (1982) 433–446.

[29] A. C. Caputo, P. M. Pelagagge, P. Salini, Heat exchanger design based on economic optimisation, Applied Thermal Engineering 28 (10) (2008) 1151–1159.

[30] A. Bejan, Convection Heat Transfer, 4th Edition, John Wiley and Sons, Inc., Hoboken, NJ, 2013.

Appendix A: Heat transfer and fluid dynamic correlations for tube and shell side fluids

The overall heat transfer coefficient $\bar{h}_{hx}$ for the tube side fluid is calculated from:

$$\bar{h}_{hx} = \frac{1}{\frac{1}{h_2} + \frac{r_{in}}{k_w}\log\left(\frac{r_{out}}{r_{in}}\right) + \frac{r_{in}}{r_{out}h_1}} \tag{10}$$

where

$$h_1 = \mathrm{Nu}_1\frac{k_1}{r_{in}}; \quad h_2 = \overline{\mathrm{Nu}_2}\frac{k_2}{r_{out}} \tag{11}$$

In addition, the turbulent Nusselt number for the tube side fluid using the friction factor [27] is taken to be

$$\mathrm{Nu}_1 = \frac{(f/8)\,(\mathrm{Re}_D - 1000)\,\mathrm{Pr}_1}{1 + 12.7\,(f/8)^{0.5}\left(\mathrm{Pr}_1^{2/3} - 1\right)} \tag{12}$$

where the friction factor is given as

$$f = \frac{1}{\left[0.790\ln\left(\mathrm{Re}_D - 1.64\right)\right]^2} \tag{13}$$

and temperature dependent Prandtl number for the tube side fluid is obtained from lookup tables.

The Nusselt number correlation for the flow through a staggered bank of tubes [30] on the shell side is given as:

$$\overline{\mathrm{Nu}_2} = A_1 C_n \mathrm{Re}_D^{n_1} \mathrm{Pr}_2^{0.36} \left(\frac{\mathrm{Pr}_2}{\mathrm{Pr}_w}\right)^{0.25} \left(\frac{a}{b}\right)^{m_1} \tag{14}$$

where A_1, n_1 and m_1 are constants as defined in Table4.

Table 4: Constants for the Nu number correlations in a tube bank at various Re_D numbers (from [30]).

Re_D	A_1	n_1	m_1
1 to 100	1.04	0.4	0.0
500 to 10^3	0.71	0.5	0.0
10^3 to 2×10^5	0.35	0.6	0.2
2×10^5 to 2×10^6	0.031	0.8	0.2

For turbulent flows, C_n has a value between 0.6 to 1, which depends on the number of tube rows in the stack as shown by Bejan [30], and a and b are dimensionless tube spacing, as depicted in Fig. 3. Reynolds number, $\mathrm{Re}_D = v_{max} D/\nu$, for the outside fluid is based on the maximum velocity through the tube banks, which occurs at the smallest cross sectional area between the tubes; and $\mathrm{Pr}_{b,w}$is evaluated for wall temperature. Further details about the approach used herein can be found in Ref. [1, 2].

Appendix B: Cost Calculations

The total heat exchanger cost is calculated using the following formula [29]:

$$C_{\text{tot}} = C_{\text{init}} + C_{\text{oper}} \tag{15}$$

$$C_{\text{init}} = 8000 + 259.2(A_m)^{0.91} = 8000 + 259.2\left(\frac{mass_m}{\rho_m t_m}\right)^{0.91} \tag{16}$$

$$C_{\text{oper}} = \left(\frac{Q_1}{\rho_1}\Delta P_1 + \frac{Q_2}{\rho_2}\Delta P_2\right)\frac{C_{\text{EL}} H_{\text{oper}}}{\eta}\left[1 - \frac{1}{(1+i)^n}\right]\frac{1}{i} \tag{17}$$

where the overall pumping efficiency, cost of electricity, operational time per year, and interest were $\eta = 1, C_{\text{EL}} = 0.2$ [\$/kW], $H_{\text{oper}} = 8,760$ [hr/year], and $i = 10\%$, respectively.